INSTITUTE OF PHYSICS PUBLISHING JOURNAL OF MICROMECHANICS AND MICROENGINEERING

J. Micromech. Microeng. **12** (2002) 219–228 PII: S0960-1317(02)29925-8

# Design and fabrication of a miniaturized, integrated, high-frequency acoustical lens–transducer system

**Jinghong Li[1], Craig R Friedrich[2] and Robert S Keynton[1,3,4]**

[1] Department of Biomedical Engineering, Louisiana Tech University, Ruston, LA, USA
[2] Department of Mechanical Engineering, Michigan Tech University, Houghton, MI, USA
[3] Department of Mechanical Engineering, University of Louisville, Louisville, KY, USA

Received 19 October 2001, in final form 7 February 2002
Published 28 March 2002
Online at stacks.iop.org/JMM/12/219

**Abstract**

High-frequency ultrasound transducers have been developed for high-resolution imaging applications, such as nondestructive testing and medical diagnostics. Several of these devices employ miniaturized acoustical lenses to enhance the resolution of the system; however, research has been limited due to lens fabrication restrictions at or below the millimeter scale, which also increases the difficulty in creating lenses of identical geometric shape. Alignment and assembly problems on the micrometer scale have also necessitated the requirement for developing an *in situ* integrated transducer–lens system. Thus, the purpose of this study was to employ a new state-of-the-art micromachining technique to fabricate a high-precision, integrated, microacoustical lens–transducer system of identical geometric shape. Concave lenses ($d = 1$ mm) were fabricated from either PMMA® or epoxy using an ultra-high-precision micromilling machine. The lenses were designed for three different focal lengths (3 mm, 4 mm or 5 mm) with a center thickness of $(3/4)\lambda$. After fabrication, each lens was evaluated for compliance with the design criteria using scanning electron microscopy and a roughness/step tester. A total of 28 lenses with identical geometry were successfully fabricated. The errors of the radii of curvatures for all PMMA® and epoxy lenses were within $7.5 \pm 5.8\%$ and $6.0 \pm 6.1\%$, respectively, of the designed values.

## 1. Introduction

High-frequency ultrasound transducers have been developed for high-resolution imaging applications, such as nondestructive testing [1–5] and medical diagnostics [6–10]. The type of focusing system employed by these systems significantly influences the accuracy, precision and sensitivity of the device. Based on the pioneering papers of Labaw [11], O'Neil [12] and Kossoff [13], the primary focusing systems developed for single-element transducers include: (1) reflectors, (2) contour emitters, (3) zone plates and (4) refractors.

Several investigators have developed acoustical lenses as a method of focusing the ultrasound beam, to reduce the lateral dimension of the beam in the focal region [14–19]. This beam narrowing decreases the size of the sample volume and increases the intensity of the ultrasound waves within the focal region, thereby, increasing the accuracy, resolution and signal-to-noise ratio (SNR) of the transducers. Several researchers have studied the effect of acoustical lenses on the centimeter scale [14–21]; however, little research has been conducted on lenses at or below the millimeter scale.

In high-frequency ultrasound, more research has been conducted in the area of refractive lenses due to the dimensional requirements associated with the design restrictions for the focusing system and ease of fabrication and/or implementation in miniaturized transducers. Ishikawa *et al* [3] developed spherical microacoustical lenses ranging

[4] Author to whom any correspondence should be addressed. Address for correspondence: Department of Mechanical Engineering, 200 Sackett Hall, University of Louisville, Louisville, KY 40292, USA.

  

from 10 to 500 $\mu$m. Their fabrication technique used air bubbles trapped inside the lens material (e.g. fused silica, quartz, flint glass and glassy carbon) during processing to construct the microspherical acoustic lens [22]. Although the surface of the lenses produced by this method possesses a mirror-like finish, the ability to produce multiple lenses of identical geometric shape is difficult; therefore, techniques must be developed whereby the lens geometry can be carefully controlled by the manufacturer. Hein [21] designed and constructed a new lens for three-dimensional (3D) flow velocity vector estimation. His design was similar to surface acoustic microscopy lenses; however, his design consisted of three lenses constructed in one rod. The beam width for each lens in the focal region was 0.5 mm and the focal length was 18.3 mm. One problem with his design was its poor SNR performance as well as significant amounts of reverberations due to the lens material (aluminum) having high acoustic impedance, which caused a significant loss of the ultrasound energy. Lalonde *et al* [19] designed a three-point focus field conjugate acoustic lens that was coupled to a 5 cm diameter PZT-5A transducer, geometrically focused at a radius of 12 cm. They selected a plastic material (polystyrene) as the lens material in order to improve the SNR. Conventional machining techniques, such as milling and lathing, were employed to fabricate these lenses; however, when the diameter of the lens was reduced to 1 mm or 2 mm, these techniques were found to be inadequate. Hartley [23] fabricated acoustical lenses for 2 mm diameter crystals using Teflon® microspheres to mold the epoxy lenses, which were later bonded to the crystal surface. This process was limited in that errors, such as a nonuniform thickness of the bonding layer, occurred while bonding the small lens to a piezoelectric crystal of similar size. In addition, both the repeatability and the precision of this technique were low.

These studies clearly indicate the limited capabilities of conventional fabrication methods and the need for alternative techniques. For example, Hashimoto *et al* [24] developed a new technique using wet chemical etching of single-crystal silicon to fabricate acoustical lenses with a diameter of 280 $\mu$m. The lenses were incorporated into a 600 MHz surface acoustic microscope (SAM), which was able to resolve lines and spaces on the order of 1.6 $\mu$m. However, similar difficulties as mentioned in the discussion in Hartley's paper were encountered in assembling, aligning and bonding the lens to the SAM system. An approach to minimize these alignment and assembly errors is to fabricate the lens *in situ* to produce an integrated transducer–lens system. Thus, the purpose of this study is to employ new state-of-the-art micromechanical machining techniques to fabricate an integrated microacoustical lens–transducer system with identical geometric configurations.

## 2. Materials and methods

In this study, a focused acoustic system was developed for implementation in a 20 MHz, high-frequency pulse ultrasonic Doppler velocimeter. The acoustic transducer material selected was lead-zirconate-titanate (PZT) due to its piezoelectric properties, high sensitivity as well as high Curie temperature, a property that insures that the piezoelectric characteristics of the material remain relatively stable at room temperature [7, 25]. Other piezoelectric materials, such as quartz and polyvinylidene difluoride, were not selected for this application due to their lower piezoelectric coefficients, sensitivity and other undesired acoustic properties [6, 25, 26].

The thickness, $\delta$, of the PZT disc should equal an integral number of one-half the wavelength in order to oscillate at the desired fundamental resonance frequency ($f$) [27, 28]

$$f = \frac{c_T}{2\delta} \tag{1}$$

where $c_T$ is the acoustic velocity in the piezoelectric material. To satisfy this relationship, chrome-gold-plated PZT-5A (Boston Piezo-Optics, Inc., Bellingham, MA) with a thickness of 100 $\mu$m was selected. Prior to fabrication, each PZT-5A crystal was evaluated for compliance to the design specifications using a roughness/step tester (RST, WYKO, Corp, Tucson, AZ) and the average thickness was found to be $100 \pm 3$ $\mu$m.

Some of the benefits of using PZT are lost due to the large acoustic mismatch between the piezoelectric and biological materials; therefore, special electrical and acoustical impedance matching must be used to reduce these losses and increase the output energy of the transducer. The acoustic velocities in the medium and lens material must differ in order to focus the acoustic beam since the differences between the indices of refraction, defined as the ratio of the acoustic velocity in material 2 to that in material 1, lead to a convergence or divergence of the acoustic beam. According to Tarnoczy [15], a concave lens utilizes less material and has lesser acoustic aberrations than a convex lens. Furthermore, the lenses should be made of a substance with a higher index of refraction than the medium and a low acoustic attenuation coefficient to maximize the energy of transmission of the transducer.

Polymethylmethacrylate (PMMA) and epoxy are often used as acoustic matching materials in low-power applications when water is the loading medium [29]. Although PMMA and epoxy attenuate the ultrasound beam more than other matching materials such as metals, their acoustic impedances are low. In this study, attenuation is not an important consideration since the transducer is designed for measuring velocities in small caliber vessels (<5 mm diameter) in close proximity to the transducer and the lens material is thin (∼0.1 mm). These materials were also selected because they are easy to machine and can be obtained in the liquid form, which will help in the fabrication of the integrated transducer–lens system.

Desilets *et al* [30] indicated that the optimum or ideal acoustic impedance, $Z_i$, of a matching material occurs when

$$Z_i = \left(Z_t Z_L^2\right)^{1/3} \tag{2}$$

where $Z_t$ is the transducer impedance and $Z_L$ is the impedance of the loading medium. For this application, the characteristic impedances of the transducer (PZT-5A) and loading medium (blood) are 29.1 MRayls and 1.6 MRayls, respectively, which result in an ideal characteristic impedance of 4.2 MRayls. Since the impedance difference between the PZT-5A and the blood is large, more than 80% of the normal incidence wave ($\theta_i = 0$) will be reflected at the interface, indicating the necessity for an impedance matching layer. Therefore, in this study, the lens material will serve not only as a focusing

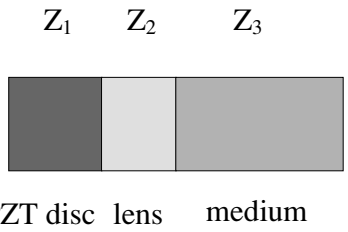


**Figure 1.** Representation of characteristic impedances $Z_1$, $Z_2$ and $Z_3$ used in equation (3).

system, but also as the impedance matching layer. While it is difficult to find a lens material that precisely satisfies the above condition, using materials with impedance values close to the ideal impedance, such as epoxy ($Z_{\text{epoxy}} = 3.8$ MRayls) and PMMA ($Z_{\text{PMMA}} = 3.2$ MRayls), will still maintain adequate bandwidth [31].

Another consideration in the design of lenses is the thickness since the lens also serves as a matching layer. The amount of energy passing through the lens material depends not only on the ratio of the acoustic impedances ($Z_1/Z_2$), but also on the ratio of the lens thickness ($d$) to the acoustic wavelength ($\lambda$). Referring to figure 1, the following expression for the amount of acoustic energy transmitted ($T$) through multiple media can be derived [32]:

$$T = \frac{4Z_3Z_1}{(Z_3+Z_1)^2\cos^2\frac{2\pi}{\lambda_2}d_2 + (Z_2+Z_3Z_1/Z_2)^2\sin^2\frac{2\pi d_2}{\lambda_2}}. \quad (3)$$

When the lens thickness $d_2$ equals $(2n–1)\lambda_2/4$ and $Z_2$ equals $(Z_1Z_3)^{1/2}$, the ratio of the energy transmitted is equal to unity, i.e. $T = 1$, which is the maximum amount of energy that can be transmitted from the transducer to the medium. When $d_2$ equals $2n\lambda_2/4$ and $Z_2$ equals $(Z_1Z_3)^{1/2}$, the ratio of the energy transmitted is equal to $4Z_1Z_3/(Z_1 + Z_3)^2$, which is the minimum amount of energy that can be transmitted.

### 2.1. Lens design

To design the concave lens, the desired focal length must first be determined (figure 2). The length of the near field of the transducer and focal length of the lens dictate the final focal length of the transducer–lens system. In addition, the diameter of the blood vessels also influences the focal length given the application of the final device. The near-field length or focal point of the transducer is determined by the acoustic wavelength ($\lambda$) in the medium and the size of the piezoelectric element [33],

$$F = r^2/\lambda \quad (4)$$

where $F$ is the focal point of the transducer and $r$ is the element radius. The pressure in the far field decreases along the axis by a factor proportional to $1/x$, where $x$ is the axial distance, and the beam in the far field diverges. The near field for the transducer used in this study is 3.25 mm since the diameter of the crystal is 1 mm, and the wavelength generated in blood (at 37 °C) is 77 $\mu$m for an operating frequency of 20 MHz. Since the operational depth of the PUDV transducer will be in the range of 1–5 mm, lens focal lengths of 3–5 mm were chosen.

If the conduction medium for ultrasound is a liquid and the lens is made from a solid material with a higher propagation velocity, the curvature of the lens must be concave to produce a converging lens. For plane–concave lenses, the focal length, $F$, can be determined using the analogy with optical lenses [33],

$$\frac{1}{F} = -\frac{1}{R}(\mu - 1) \quad (5)$$

where $\mu = c_1/c_2$, $R$ is the radius of curvature, $\mu$ is the index of refraction of the lens material related to the environment, $c_1$ is the acoustic velocity of the medium and $c_2$ is the acoustic velocity of the lens material. Using this relationship, the radii of curvature (ROC) of the lenses were calculated for each focal length (table 1). A center lens thickness of $(3/4)\lambda$ was chosen for maximum acoustic transmission and for providing an adequate amount of material for proper coverage of the lead wires on the top surface of the transducer.

Tarnoczy [15] has also demonstrated that a circular transducer combined with an acoustical lens will result in a transducer–lens system with a focal length of [34]

$$\frac{1}{f_1} + \frac{1}{f_2} - \frac{d}{f_1 f_2} = \frac{1}{F} \quad (6)$$

where $f_1$ is the focal length of the crystal, $f_2$ is the focal length of the lens, $F$ is the focal length of the combined system and $d$ is the distance between the crystal and the lens. In this study, $d$ was equal to the center thickness of the lenses which was ~0.1 mm.

### 2.2. Fabrication

Prior to the lens fabrication process, a specially designed holding well was fabricated to secure the transducer–lens system in place during the micromilling process (figures 3 and 4). The holding well was fabricated using a custom-built, ultra-high-precision micromilling machine and Teflon® was selected as the holding well material because of its nonstick properties, machinability and low thermal expansion coefficient. A total of 18 through holes ($d = 0.9$ mm) were machined in two rows (nine holes per row) with a 5 mm spacing between each hole in a 60 mm × 110 mm Teflon® base. Counter sink holes ($d = 1.1$ mm) were then machined in the through holes to depths equal to the thickness of the lens edge ($h + (3/4)\lambda$) and the crystal thickness ($t = 100 \pm 3\,\mu$m) (table 2). With each hole, a 20 mm × 0.5 mm × 0.2 mm trench was milled in the Teflon® to act as a guide for the wire leads.

Prior to placing the crystal in the holding well, two strands of 50 $\mu$m silver wire (Cooner Wire, Chatswood, CA) were braided together and bonded to the top surface of the crystal using conductive silver epoxy (Hosfelt Electronics, Inc., Steubenville, OH). A transducer-wire ensemble was placed in each of the 1.1 mm counter sink holes and rested on the lip of the 0.9 mm through hole. Each holding well was then filled with one of the two lens materials. The epoxy lens material required mixing prior to application, which consisted of combining five parts epoxy resin (Plast 88, E.I. DuPont Co, Wilmington, DE) with one part of epoxy hardener (Plast 87, E.I. DuPont Co, Wilmington, DE). Following mixing, the epoxy was placed inside a vacuum chamber to remove the air bubbles from the mixture. Subsequently, the epoxy mixture was placed on the surface of the crystals which were placed in each hole for one-half of the holding well (nos 10–18).

**Table 1.** Summary of design data for the microlenses.

| | Focal length (mm) | Focal length of lens system (mm) | Radii of curvature (mm) | Designed depth $h$ ($\mu$m) | Center thickness $d$ ($\mu$m) | Velocity (m s$^{-1}$) |
|---|---|---|---|---|---|---|
| Epoxy | 3 | 1.61 | 1.427 | 90.5 | 108.7 | 2898 |
| | 4 | 1.85 | 1.902 | 66.9 | | |
| | 5 | 2.03 | 2.378 | 53.2 | | |
| PMMA | 3 | 1.61 | 1.283 | 101.5 | 100.9 | 2690 |
| | 4 | 1.85 | 1.710 | 74.7 | | |
| | 5 | 2.03 | 2.138 | 59.3 | | |

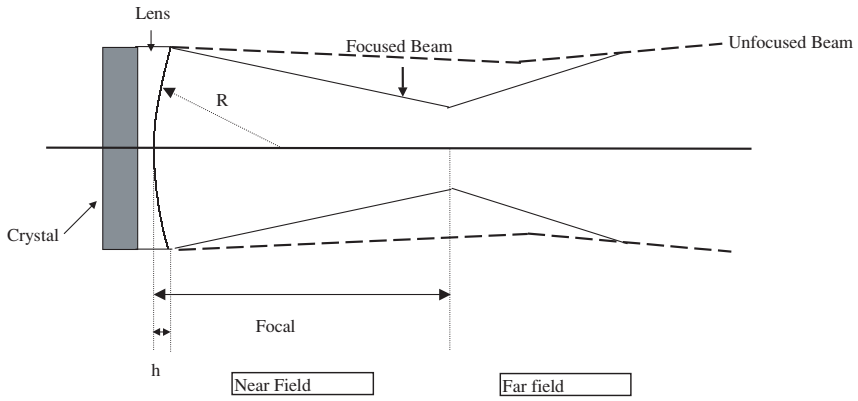


**Figure 2.** Schematic of the microlens design (adapted from [27]). $R$ is the radius of curvature of the lens surface and $h$ is the edge thickness of the lens.

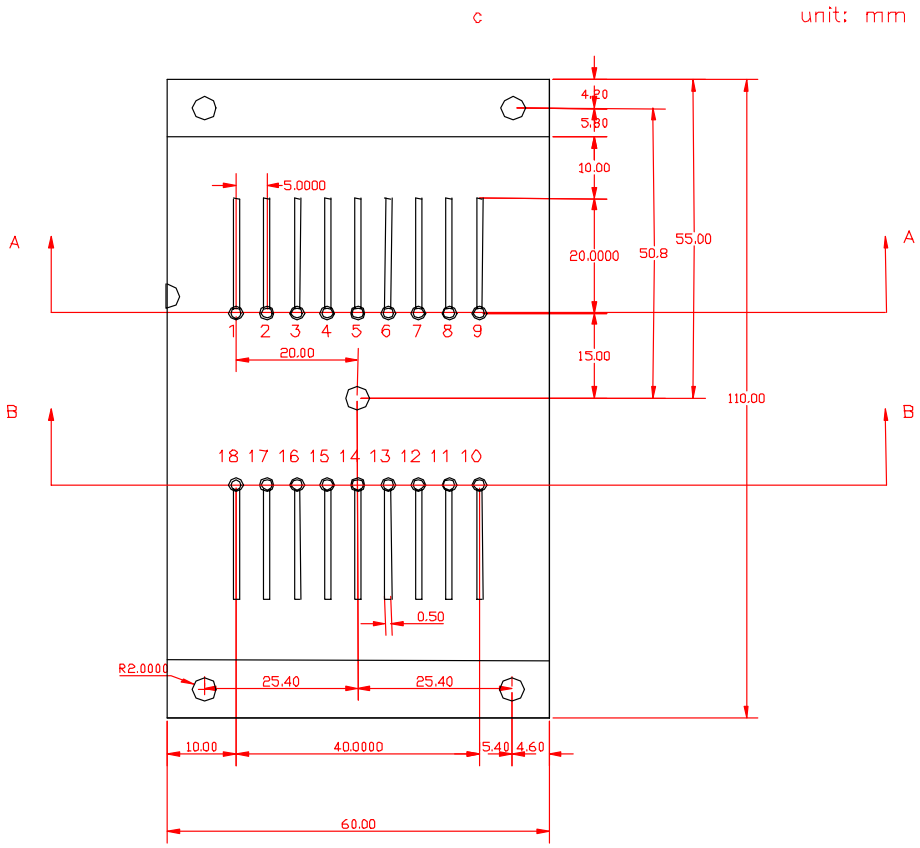


**Figure 3.** Design drawing of the holding well (top view). Note: all slots have width 0.5 mm, depth 0.2 mm and all screw holes have the same diameter.

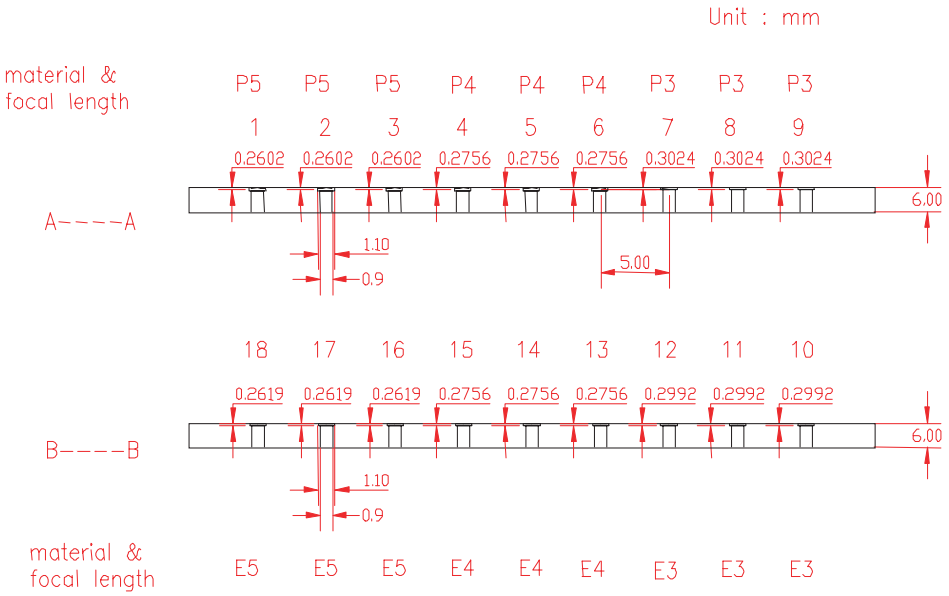


**Figure 4.** Design drawing of the holding well (side view).

**Table 2.** The depth of the counter sink holes machined in the Teflon® holding well.

| Hole number | Focal length | Well depth ($\mu$m) |
|---|---|---|
| 1–3 | PMMA (5 mm) | 260.2 |
| 4–6 | PMMA (4 mm) | 275.6 |
| 7–9 | PMMA (3 mm) | 302.4 |
| 10–12 | Epoxy (3 mm) | 299.2 |
| 13–15 | Epoxy (4 mm) | 275.6 |
| 16–18 | Epoxy (5 mm) | 261.9 |

The holding well was then placed in a curing oven set at a temperature of 55 °C for 24 h. After curing the epoxy, the remaining nine holes (nos 1–9) were filled with PMMA dissolved in methylene chloride. Finally, the holding well was again placed in the curing oven set at a temperature of 45 °C for 24 h.

After the curing process, the holding well was placed in a custom-made ultra-high-precision micromilling machine. The micromilling machine consisted of an air spindle operating at a speed of 6000 RPM and a laser-controlled positioning system with air bearings [35]. The positioning system has a translational resolution of ∼1 nm in the $x$- and $y$-directions and 20 nm resolution in the $z$-direction. The top surface of each lens was first planed down to the top surface of the holding well using a 2 mm diameter end-mill. This step provided a common reference point for the top surface of each lens. Subsequently, the curvatures of the lenses were machined via a step-wise process, as shown in figure 5, using a 100 $\mu$m diameter end-mill. A custom-made computer program, written in G-code, was developed to control the step-wise machining process. The milling process consisted of traversing the 'work table' in a circular fashion starting with a 500 $\mu$m radius. Each concentric ring was machined in 10 $\mu$m steps from the outer edge of the lens. The depth of the cut ($d$) was determined using the following formula

$$d = \sqrt{R^2 - (r_c - 10)^2} - \sqrt{R^2 - r_c^2} \qquad (7)$$

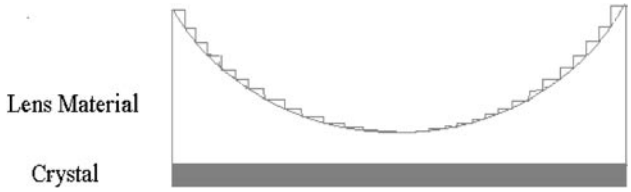


**Figure 5.** Schematic view of the step-wise milling process.

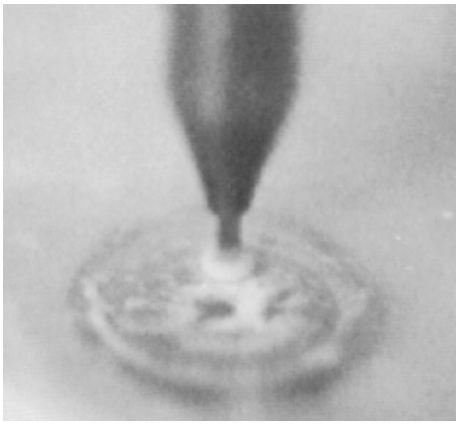

**Figure 6.** Milling process in use. The tool was 100 $\mu$m in diameter. The concentric pattern was seen under the tool (magnification = 10×).

where $R$ is the radius of curvature and $r_c$ is the radius of the previously machined concentric layer. Therefore, the degree of concavity and maximum depth of concavity were varied depending on the lens design. This process was repeated until the radius of the concentric layer reached 50 $\mu$m, which corresponded to the radius of the tool, resulting in a total of 45 concentrically milled layers (figures 5 and 6).

### 2.3. Metrology

Qualitative analysis of the lens surface was performed using a scanning electron microscope (SEM) (AMRAY, Inc., Santa

Clara, CA) and an optical microscope (Optistation, Nikon, Tokyo, Japan). Surface images were obtained using both 5× and 20× objectives to obtain a full field-of-view and regional images of the lens surface, respectively. The radii of curvature, center thickness and dimensions of each lens were quantified using a roughness/step tester (RST, WYKO, Corp, Tucson, AZ). The RST was operated in the vertical scanning interferometry mode to profile the lens surface. At evenly spaced intervals during the scan, frames of the interference data were imaged by the video camera, captured and processed by the software. The system profiled the surface using a root-mean-square (rms) roughness term, $R_q$,

$$R_q = \sqrt{\frac{1}{N}\sum_{i=1}^{N}|Z_i - Z|^2} \tag{8}$$

where $N$ is the number of data points between two designated cursors, $Z_i$ is the point-by-point height deviation between the measured profile and the mean line, and $Z$ is the reference mean line. The RST system can measure a rms roughness ranging from 10 Å to 200 $\mu$m. In addition, the arithmetic average roughness, $R_a$, was also obtained using the following relationship [36]

$$R_a = \frac{1}{N}\sum_{i=1}^{N}|Z_i - Z|. \tag{9}$$

Prior to conducting the RST measurements, a 1–5 nm layer of gold or chrome was sputtered on the epoxy lens surfaces to enhance the amount of reflection for the RST measurement. The objective used for the RST measurement was 5×, which provided a field view of 1.2 mm × 0.9 mm.

Figure 7 illustrates the output obtained and displayed by the RST. Figure 7(*a*) is an example of a typical lens surface as represented by the RST. The graphs (*b*) and (*c*) demonstrate typical profiles produced by the RST along the *x*- and *y*-axes, respectively. The depth measurement was obtained by placing one cursor at the edge of the lens and positioning a second cursor at the center (or lowest point) of the profile. The difference, $D$, of these two locations was computed as the depth of the lens.

The radius of curvature (ROC) was computed as the average ROC obtained from the data points between the two cursors positioned in the depth measurement. The ROC of each point was determined by

$$\mathrm{ROC} = \frac{\mathrm{d}^2 z}{\mathrm{d}r^2} \tag{10}$$

where $r$ is the radius and $z$ is the height. All ROC, surface roughness and center thickness measurements were repeated three times to obtain an average (±SD) value.

After RST evaluation, the transducer–lens systems were removed from the holding well and two strands of 50 $\mu$m silver wire were braided together and bonded to the back side of the piezoelectric crystals to supply a ground to the transducer. Heat shrinking tubing was placed around each wire lead to protect the wires from mechanical damage. The wire leads were attached to a coaxial cable (RG174, $R = 50\ \Omega$) with the top lead wire silver soldered to the copper core and the bottom lead wire silver soldered to the shielding layer of the cable. Subsequently, the wire leads and coaxial cable were fed

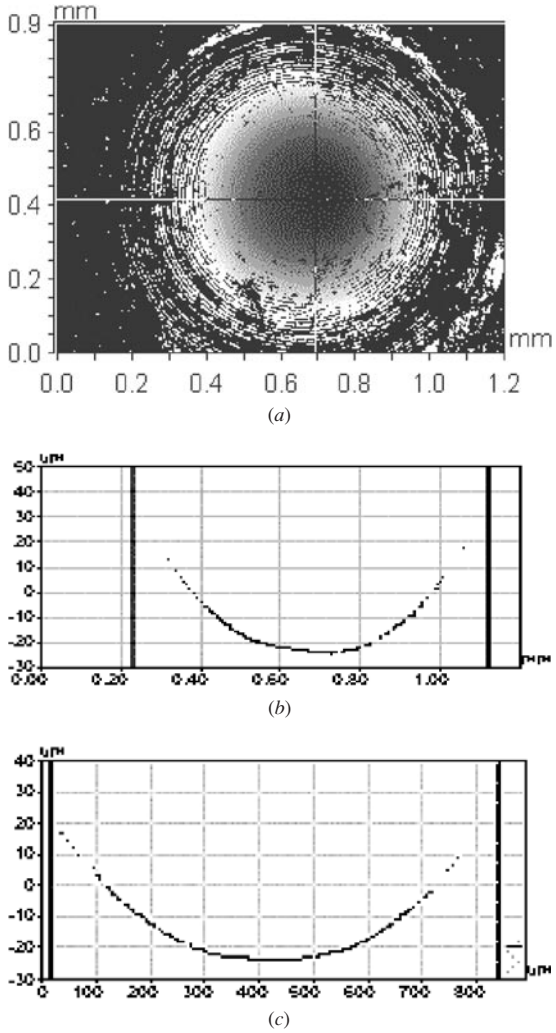


**Figure 7.** Video display of the output from the RST: (*a*) image of the lens surface, (*b*) profile along the center-line of the *x*-axis and (*c*) profile along the center-line of the *y*-axis.

through a 76 mm long brass tube (OD = 3.2 mm; ID = 2.4 mm) to protect the transducer and wires from mechanical damage. The tip of the brass tube was back-filled with a composite of epoxy impregnated with 50 $\mu$m tungsten particles (50% by weight). This high-impedance acoustic backing material (6–16 MRayls) eliminated 'ringing effects' and optimized the pulse length and bandwidth of the transducer [37].

## 3. Results

### *3.1. Qualitative lens analysis*

A total of 28 microlenses were successfully fabricated; 13 made of PMMA and 15 made of epoxy (table 3). Qualitative analysis of the lenses was performed, by obtaining SEM images at 70× magnification. The surface concavity of the lenses is illustrated in these images (figures 8 and 9) as well as the quality of integration between the crystal and the lens material.

Following SEM imaging, the lenses were inspected with an optical microscope to qualitatively view features on the top surface (figures 10 and 11). Figure 10 shows a

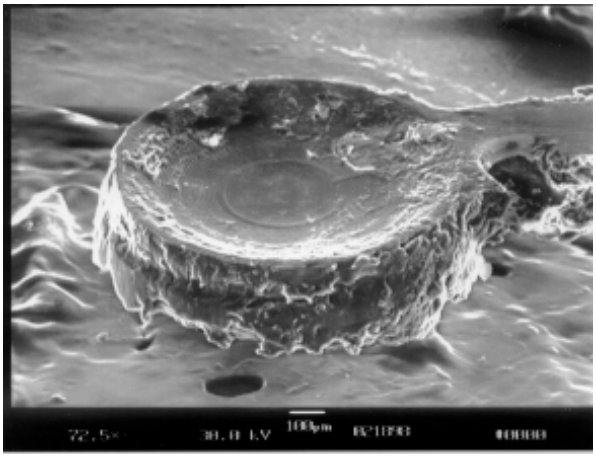

**Figure 8.** A SEM view of a PMMA lens (lens P2). The designed radius of curvature of this lens was 1.28 mm and the diameter of the lens was 1 mm. The scale bar was 100 $\mu$m.

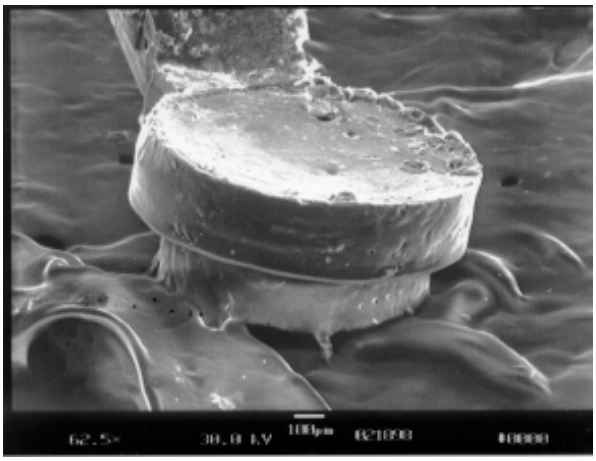

**Figure 9.** A SEM view of an epoxy lens (lens E6). The designed radius of curvature of this lens was 1.90 mm and the diameter of the lens was 1 mm. The scalar bar was 100 $\mu$m.

field-of-view of the entire lens surface, illustrating the concentric rings produced during the machining process. Figure 11 is a magnification of the lens and provides a more detailed view of the concentric rings on the surface. Each ring corresponded to a step and the surface of each step appeared smooth and uniform. Epoxy lenses were also viewed with the optical microscope; however, since epoxy is not a good light reflecting material, a chrome coating had to be applied to image the epoxy lens surface (figure 12).

### *3.2. Quantitative lens analysis*

The average $R_a$ and $R_q$ for all PMMA lenses were 1.41 $\pm$ 0.49 $\mu$m and 1.82 $\pm$ 0.51 $\mu$m, respectively (table 3). The average $R_a$ and $R_q$ for all epoxy lenses were 1.36 $\pm$ 0.60 $\mu$m and 1.74 $\pm$ 0.71 $\mu$m, respectively (table 3). Using an independent *t*-test, assuming equal variance, it was found that between groups, the roughnesses for PMMA lenses and epoxy lenses were not significantly ($\alpha = 0.05$) different.

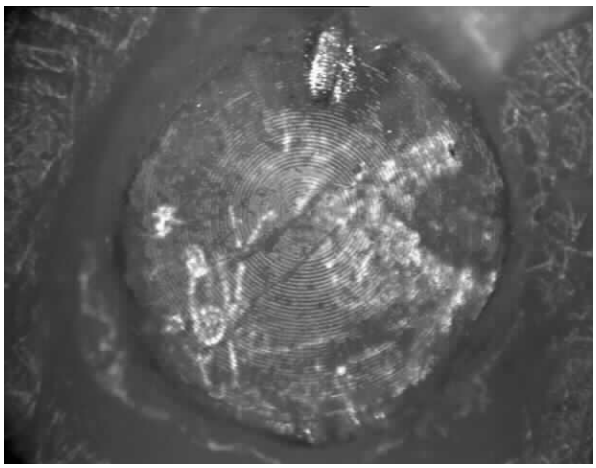

**Figure 10.** An optical microscope view of a PMMA lens with a 5$\times$ objective.

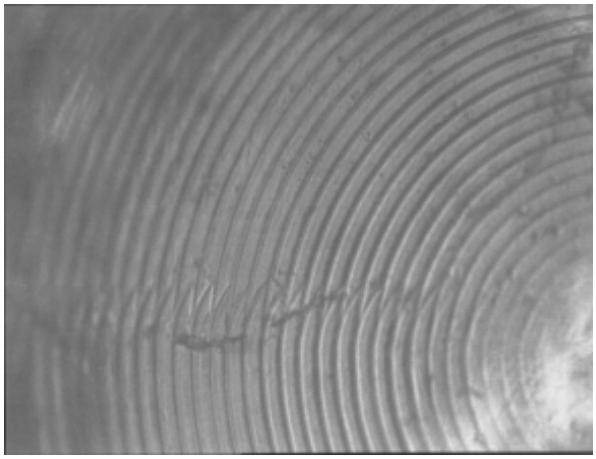

**Figure 11.** An optical microscope view of a PMMA lens with a 20$\times$ objective.

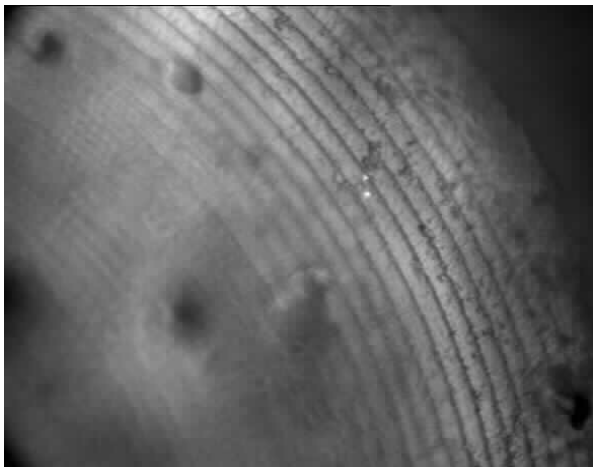

**Figure 12.** An optical microscope view of an epoxy lens with a 20$\times$ objective.

### *3.3. Radius of curvature*

For the PMMA lenses, the measured radii of curvature were within 10.5 $\pm$ 6.3%, 4.6 $\pm$ 2.2% and 5.3 $\pm$ 6.6% of the designed value for each group (table 4). For the epoxy lenses,

**Table 3.** Average surface roughness of the epoxy and PMMA lenses.

| | Focal length (mm) | Number of lenses averaged $N$ | $R_a$ mean ± SD ($\mu$m) | $R_q$ mean ± SD ($\mu$m) |
|---|---|---|---|---|
| Epoxy | 3 | 5 | 1.046 ± 0.489 | 1.417 ± 0.644 |
| | 4 | 5 | 1.535 ± 0.745 | 1.951 ± 0.852 |
| | 5 | 5 | 1.488 ± 0.558 | 1.864 ± 0.619 |
| PMMA | 3 | 6 | 1.187 ± 0.430 | 1.568 ± 0.446 |
| | 4 | 4 | 2.235 ± 0.769 | 2.873 ± 0.787 |
| | 5 | 3 | 0.773 ± 0.224 | 0.935 ± 0.247 |

**Table 4.** Radius of curvature for the epoxy and PMMA lenses.

| | Focal length (mm) | Number of lenses averaged $N$ | Measured radius of curvature (mm) | Error (%) |
|---|---|---|---|---|
| Epoxy | 3 | 5 | 1.538 ± 0.146 | 7.470 ± 8.783 |
| | 4 | 5 | 1.986 ± 0.118 | 4.438 ± 3.025 |
| | 5 | 5 | 2.528 ± 0.146 | 6.186 ± 6.126 |
| PMMA | 3 | 6 | 1.417 ± 0.142 | 10.470 ± 6.278 |
| | 4 | 4 | 1.790 ± 0.115 | 4.593 ± 2.226 |
| | 5 | 3 | 2.253 ± 0.167 | 5.267 ± 6.623 |

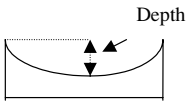


**Figure 13.** Schematic of the definition of the depth measurement.

the measured radii of curvature were within 7.5 ± 8.8%, 4.4 ± 3.0% and 6.2 ± 6.1% of the designed value for each group (table 4). The overall error for the PMMA lenses was 7.5 ± 5.8%, and 6.0 ± 6.1% for the epoxy lenses. Assuming equal variance, the independent *t*-test of the errors showed that the radii of curvatures for the PMMA and epoxy lenses were not significantly ($\alpha = 0.05$) different.

### *3.4. Lens thickness*

The depth of concavity was measured in order to calculate the center thickness of the lens. The depth was defined as the vertical distance from the outer edge of the lens to the surface of the lens center (figure 13). The error of the measured depth for the PMMA lenses was within –4.5 ± 7.2% of the design and the error for the epoxy lenses was within 8.0 ± 8.4% (table 5). An independent *t*-test was performed on the errors of the depth for the PMMA and epoxy lenses and it was found that the material did differ significantly ($\alpha = 0.01$).

The center thickness of the lenses could not be directly measured; therefore, the center thickness was calculated from the depth measurement data. The center thickness of the lens is equal to the depth of the holding well minus the sum of the crystal thickness and lens depth. The average thickness of the crystals was 100 ± 3 $\mu$m, and the well depth was different for each lens since the well depth depended upon both the focal length and the type of material.

For the PMMA lenses, the average center thickness of all the lenses was 104.0 ± 6.2 $\mu$m while the mean value for the epoxy lenses was 103.2 ± 5.9 $\mu$m (table 6). The errors

**Table 5.** The depth of the epoxy and PMMA lenses.

| | Focal length (mm) | Number of lenses averaged $N$ | Measured depth ($\mu$m) | Error (%) |
|---|---|---|---|---|
| Epoxy | 3 | 5 | 96.20 ± 2.66 | 6.3 ± 8.5 |
| | 4 | 5 | 73.78 ± 1.66 | 10.3 ± 8.2 |
| | 5 | 5 | 57.18 ± 1.42 | 7.5 ± 9.7 |
| PMMA | 3 | 6 | 101.93 ± 3.08 | 0.4 ± 7.0 |
| | 4 | 4 | 66.30 ± 1.83 | −11.2 ± 1.1 |
| | 5 | 3 | 56.23 ± 2.10 | −5.2 ± 4.4 |

**Table 6.** The center thickness of the epoxy and PMMA lenses.

| | Focal length (mm) | Number of lenses averaged $N$ | Calculated center thickness ($\mu$m) | Error (%) |
|---|---|---|---|---|
| Epoxy | 3 | 5 | 103.7 ± 7.7 | –5.2 ± 7.1 |
| | 4 | 5 | 101.8 ± 5.5 | –6.3 ± 5.0 |
| | 5 | 5 | 104.7 ± 5.2 | –3.7 ± 4.7 |
| PMMA | 3 | 6 | 101.5 ± 7.1 | –0.4 ± 7.1 |
| | 4 | 4 | 109.3 ± 0.8 | 8.3 ± 0.8 |
| | 5 | 3 | 104.0 ± 2.6 | 3.1 ± 2.6 |

of the center thickness for all the lenses were within 2.2 ± 10.0%. The center thickness of the PMMA lenses and epoxy lenses was found to be within 3.1 ± 6.1% and –5.1 ± 5.4%, respectively, of the designed values. Again, the two materials were found to vary significantly ($\alpha = 0.01$).

## 4. Discussion

Overall, the surface roughness for all the lenses was within 1.8 ± 0.7 $\mu$m (table 3). Optimally, a smooth lens surface is desired since a smooth surface will reduce the amount of refraction occurring at the interface. A higher surface roughness will alter the effect of the lens on the ultrasound beam by increasing the amount of refraction at the lens surface. For example, lenses E6 and P8 had surface roughnesses significantly ($\alpha = 0.01$) higher than the other lenses and these lenses also yielded some of the largest errors (62% and 41%, respectively) for the beam width estimations. (Note that all transducer–lens systems were characterized using a Schlieren system. The results of this study have been presented in a subsequent report [38].) These discrepancies may be due to several factors. Firstly, the machining process, in and of itself, introduces a roughness of 5–10 $\mu$m due to the step-wise process. These steps were incorporated within the RST measurements as part of the surface roughness. Secondly, some material residues remained on the surface of the lens due to improper cleaning of the lens surface following the fabrication process. These residues resulted in an increase in the surface roughness. Finally, in the case of epoxy, the 1–5 nm layer of gold or chrome deposited on the surface affected the roughness by covering the step surface with variable thickness, clearly affecting the average roughness.

The intrinsic properties of the material, e.g. hardness, may also affect the surface roughness. For example, epoxy was a softer material than PMMA and deformed more easily; thus,

bubbles would attenuate the acoustic intensity and alter the beam pattern.

## 5. Conclusions

A total of 28 acoustical lenses with specially designed radii of curvatures were successfully fabricated in this study. The holding well designed in this study enabled the construction of an integrated transducer–lens system. The errors for the radii of curvatures and center thickness were within $\pm 14\%$ and $\pm 11\%$, respectively, of the designed values. The radii of curvature were found to be within $\pm 2\sigma$ for both lens materials and the radii of curvatures for the PMMA lenses and epoxy lenses within each respective group were not significantly ($\alpha = 0.05$) different. Therefore, the micromilling machine demonstrates the capability of fabricating high-precision microlenses of identical geometric configuration.

## Acknowledgments

The authors would like to thank Richard Miles and Julie Amaden for their technical assistance in this project. We also wish to gratefully acknowledge the financial support of the National Science Foundation (contract no NSF/LEQSF(1995–98)-SI-01), the Department of Defence (no DAAH04-96-1–0200) and Indus Instruments, Inc., Houston, TX, in this research endeavor.

## References

[1] Kushibiki J and Chubachi N 1985 Material characterization by line-focus-beam acoustic microscope *IEEE Trans. Sonics Ultrason.* **32** 189–212

[2] Moulthrop A A, Muha M S, Hadimioglu B, Silva C P and Kozlowski G C 1992 Acoustic microscopy and nonlinear effects in pressurized superfluid helium *IEEE Trans. Ultrason. Ferroelectr. Freq. Control* **39** 204–11

[3] Ishikawa I, Kanda H and Katakura K 1985 An acoustic microscope for subsurface defect characterization *IEEE Trans. Sonics Ultrason.* **32** 325–31

[4] Foster F S, Pavlin C J, Lockwood G R, Ryan L K, Harasiewicz K, Berube L and Rauth A M 1993 Principles and applications of ultrasound backscatter microscopy *IEEE Trans. Ultrason. Ferroelectr. Freq. Control* **40** 608–16

[5] Semba T, Tani Y and Sato H 1993 Material characterization of a machined surface using an anisotropic acoustic lens *CIRP Ann.* **42** 627–30

[6] Sherar M D and Foster F S 1989 The design and fabrication of high frequency poly(vinylidene fluoride) transducers *Ultrason. Imaging* **11** 75–94

[7] Lockwood G R, Turnbull D H and Foster F S 1994 Fabrication of high frequency spherically shaped ceramic transducers *IEEE Trans. Ultrason. Ferroelectr. Freq. Control* **41** 231–5

[8] Foster F S, Ryan L K and Turnbull D H 1991 Characterization of lead zirconate titanate ceramics for use in miniature high frequency (20–80 MHz) transducers *IEEE Trans. Ultrason. Ferroelectr. Freq. Control* **38** 446–53

[9] Passmann C and Ermert H 1996 A 100-MHz ultrasound imaging system for dermatologic and ophthalmologic diagnostics *IEEE Trans. Ultrason., Ferroelectr. Freq. Control* **43** 545–52

[10] Pavlin C J and Foster F S (ed) 1995 *Ultrasound Biomicroscopy of the Eye* (Berlin: Springer)

[11] Labaw L W 1945 Curved quartz crystal as supersonic generators 1945 *J. Acoust. Soc. Am.* **16** 237–45

[12] O'Neil H T 1949 Theory of focusing radiators *J. Acoust. Soc. Am.* **21** 516–26

[13] Kossoff G 1963 Design of narrow-beamwidth transducers *J. Acoust. Soc. Am.* **35** 905–12

[14] Golis M J 1968 An analysis of the ultrasonic zone lens *IEEE Trans. Sonics Ultrason.* **15** 105–10

[15] Tarnoczy T 1965 Sound focusing lenses and waveguides *Ultrasonics* **3** 115–27

[16] Lewin P A 1981 Miniature piezoelectric polymer ultrasonic hydrophone probes *Ultrasonics* **19** 213–6

[17] Hein I A 1995 Triple-beam lens transducers for three-dimensionally ultrasonic fluid flow estimation *IEEE Trans. Ultrason. Ferroelectr. Freq. Control* **42** 854–69

[18] Pappalardo M 1981 Hybrid linear and matrix acoustic array *Ultrasonics* **19** 81–6

[19] Lalonde R J, Worthington A and Hunt J W 1993 Field conjugate acoustic lenses for ultrasound hypothermia *IEEE Trans. Ultrason. Ferroelectr. Freq. Control* **40** 592–602

[20] Szilard J and Kidger M 1976 A new ultrasonic lens *Ultrasonics* **14** 268–72

[21] Hein I A 1995 3-D blood flow velocity vector estimation with a triple-beam lens—experimental results *IEEE Ultrason. Symp.* **2** 1471–6

[22] Ishakawa I, Kanda H and Kondoh T 1983 Acoustic spherical lens and method of manufacturing *US Patent* 4 384 231

[23] Hartley 1996 Personal communication

[24] Hashimoto H, Tanaka S, Sato K, Ishikawa I, Kato S and Chubachi N 1993 Chemical isotropic etching of single-crystal silicon for acoustic lens of scanning acoustic microscope *Japan. J. Appl. Phys.* **32** 2543–6

[25] Hunt J W, Arditi M and Foster F S 1983 Ultrasound transducers for pulse-echo medical imaging *IEEE Trans. Biomed. Eng.* **30** 453–81

[26] Sleva M Z, Briggs R D and Hunt W D 1996 A micromachined poly(vinylidene fluoride-trifluoroethylene) transducer for pulse-echo ultrasound applications *IEEE Trans. Ultrason. Ferroelectr. Freq. Control* **43** 257–62

[27] Wells P N T 1977 *Biomedical Ultrasonics* (New York:Academic)

[28] Parker S P 1988 *Acoustic Source Book* (New York:McGraw-Hill)

[29] Stanley R C 1968 *Light and Sound for Engineers* (New York: Hart Publishing Company)

[30] Desilets C S Fraser J D and Kino G S 1978 The design of efficient broad-band piezoelectric transducers *IEEE Trans. Sonics Ultrason.* **25** 115–25

[31] Bronzino J D (ed) 2000 *The Biomedical Engineering Handbook* 2nd edn vol 1 (Danvers, MA: CRC Press LLC and IEEE Press)

[32] Kinsler L E and Frey A R 1962 *Fundamentals of Acoustics* (New York: Wiley)

[33] Shung K K, Smith M B and Tsui B M W 1992 *Principles of Medical Imaging* (San Diego, CA: Academic) pp 78–159

[34] Dusseldorf V 1971 Toepler's Schlieren method—basic principles for its use and quantitative evaluation, Selected paper on Schlieren Optics

[35] Friedrich C R and Vasile M J 1996 Develeopment of the micromilling process for high aspect ratio microstructures *J. MEMS* **5** 33–8

[36] *Analysis of Material Removal Processes* 1997 ed W R DeVries and F F Ling (New York: Springer)

[37] Grewe M G, Gururaja T R, Shrout T R and Newnham R E 1990 Acoustic properties of particle/polymer composites for ultrasonic transducer backing applications *IEEE Trans. Ultrason. Ferroelectr. Freq. Control* **37** 506–14

[38] Li J, Friedrich C R and Keynton R S 2001 Performance evaluation of an integrated, high frequency acoustical lens-transducer system *IEEE Trans. Ultrason. Ferroelectr. Freq. Control* submitted